

Electronic structure of self-assembled InAs/InP quantum dots: A Comparison with self-assembled InAs/GaAs quantum dots

Gong Ming,¹ Kaimin Duan,¹ Chuan-Feng Li,¹ Rita Magri,² Gustavo A. Narvaez,³ and Lixin He ^{*1}

¹*Key Laboratory of Quantum Information, University of Science and Technology of China, Hefei, 230026, People's Republic of China*

²*Cnism-CNR and Dipartimento di Fisica, Università di Modena e Reggio Emilia, Via Campi 213/A, 41100 Modena, Italy*

³*Amin, Turocy & Calvin, LLP, Cleveland, OH 44114, USA*

(Dated: February 8, 2022)

We investigate the electronic structure of the InAs/InP quantum dots using an atomistic pseudopotential method and compare them to those of the InAs/GaAs QDs. We show that even though the InAs/InP and InAs/GaAs dots have the same dot material, their electronic structure differ significantly in certain aspects, especially for holes: (i) The hole levels have a much larger energy spacing in the InAs/InP dots than in the InAs/GaAs dots of corresponding size. (ii) Furthermore, in contrast with the InAs/GaAs dots, where the sizeable hole p , d intra-shell level splitting smashes the energy level shell structure, the InAs/InP QDs have a well defined energy level shell structure with small p , d level splitting, for holes. (iii) The fundamental exciton energies of the InAs/InP dots are calculated to be around 0.8 eV ($\sim 1.55 \mu\text{m}$), about 200 meV lower than those of typical InAs/GaAs QDs, mainly due to the smaller lattice mismatch in the InAs/InP dots. (iii) The widths of the exciton P shell and D shell are much narrower in the InAs/InP dots than in the InAs/GaAs dots. (iv) The InAs/GaAs and InAs/InP dots have a reversed light polarization anisotropy along the $[100]$ and $[1\bar{1}0]$ directions.

PACS numbers: 68.65.Hb, 73.22.-f, 78.67.Hc

I. INTRODUCTION

Self-assembled semiconductor quantum dots (QDs) have attracted a large interest because the discrete and isolated energy levels due to the 3D confinement can be utilized in high-efficiency and low-threshold current lasers,^{1,2,3,4} single photon emitters^{5,6} and in quantum computing applications (qubits).^{7,8} $1.3 \mu\text{m}$ optical devices have been achieved using InAs/GaAs quantum dots,^{2,3,9} however, it is difficult to push further the InAs/GaAs QD devices to work at the more desirable $\sim 1.55 \mu\text{m}$ telecommunication wavelength because the large compressive strain (7%) in the InAs/GaAs dots enlarges the conduction-valence energy gap of InAs too much for this purpose. Intuitively, a InAs dot embedded in a less lattice mismatched host material, e.g. InP, should solve the problem. Indeed, recently there have been reports on $1.55 \mu\text{m}$ InAs/InP QDs lasers with a high-gain and a low-threshold current,^{1,10} which opens up the possibility to integrate quantum dot material into an optical cavity¹¹ and hence to reliably fabricate a single photon source in the telecommunications wavelength range.^{5,6}

Despite their importance, there are only few studies on the InAs/InP system, both theoretically^{12,13} and experimentally^{14,15,16,17,18,19} compared to the well studied InAs/GaAs QDs. Although the InAs/InP dots and the InAs/GaAs dots have the same dot material, they differ in three aspects, (i) InAs/InP has a much smaller

lattice mismatch (3%) than InAs/GaAs (7%). (ii) The InAs/InP dots have a less confining potential for electrons, but a stronger confinement for holes than the InAs/GaAs dots. (iii) The InAs/InP dots share the same cation (In), while the InAs/GaAs QDs share the same anion (As) at the interface. These differences may lead to different electronic and optical properties of the two systems. The continuum theories, such as those based on the effective mass approximation (EMA) and multi-bands $\mathbf{k} \cdot \mathbf{p}$ method, may in principle capture the first two differences, however, to account for the third aspect, one needs atomistic theories such as the empirical pseudopotential methods^{20,21} or the tight-binding methods.^{12,22} The empirical pseudopotential methods have been successfully applied to various systems.^{21,23} In this paper, we perform a comparative study on the InAs/InP QDs and InAs/GaAs QDs using an atomistic pseudopotential method. We find that there are significant differences in the electronic structure between the two systems, including the single-particle energy levels and optical properties. These differences, which have not yet been paid enough attention to, could be revealed in the future high-resolution optical spectroscopy^{24,25} and charging experiments.^{26,27}

The rest of the paper is organized as follows. In Sec. II, we introduce briefly the atomistic pseudopotential method used in the calculations. In Sec. III, we compare the strain profiles and the strain modified band-offsets for the InAs/GaAs and InAs/InP QDs. In Sec. IV, we compare the pseudopotential calculated electronic structure as well as the wavefunctions of the two dots. We compare the excitonic transitions of the two dots in Sec. V and conclude in Sec. VI.

*corresponding author: helx@ustc.edu.cn

II. METHODS

The geometries of the QDs studied here are lens-shaped InAs dots embedded in the host materials (GaAs or InP) matrices containing $60 \times 60 \times 60$ 8-atom unit cells. The dots are assumed to grow along the [001] direction. We performed the calculations on dots with base diameters $D=20$, and 25 nm, and for each base diameter, we vary the dot heights h from 2.5 nm to 5.5 nm, as the dot height is relatively easy to control in experiments.²⁸ We first relax the dot+matrix system by minimizing the strain energy as a function of the coordinate $\{\mathbf{R}_{n,\alpha}\}$ of atom α at site n for all atoms, using valence force field (VFF) methods.^{29,30} Once we have the atom positions, we obtain the energy levels and wavefunctions by solving the single-particle Schrödinger equation,

$$\left[-\frac{1}{2}\nabla^2 + V_{ps}(\mathbf{r})\right] \psi_i(\mathbf{r}) = \epsilon_i \psi_i(\mathbf{r}), \quad (1)$$

where $V_{ps}(\mathbf{r}) = V_{SO} + \sum_n \sum_\alpha v_\alpha(\mathbf{r} - \mathbf{R}_{n,\alpha})$ is the superposition of local screened atomic pseudopotentials $v_\alpha(\mathbf{r})$, and the total (non-local) spin-orbit (SO) potential V_{SO} . The screened pseudopotentials²¹ are fitted to the physical important properties of the materials, including the band energies at high-symmetry points, effective masses, strained band offsets, hydrostatic and biaxial deformation potentials of individual band edges. The pseudopotentials of InAs/InP dots are given in Appendix A, whereas the potentials for InAs/GaAs QDs are taken from Ref. 21. The Schrödinger Eq. (1) is solved by expanding the wavefunctions ψ_i as linear combinations of bulk bands (LCBB)²⁰ $\{\phi_{m,\vec{\epsilon},\lambda}(\mathbf{k})\}$ of band index m and wave vector \mathbf{k} of material λ ($=$ InAs, GaAs, InP), strained uniformly to strain $\vec{\epsilon}$. We use $m=2, 3, 4$ for the hole states, and $m=5$ for electron states on a $6 \times 6 \times 16$ k-mesh. We use $\vec{\epsilon} = 0$ for the matrix material, and an average $\vec{\epsilon}$ value from VFF for the strained dot material (InAs). It has been shown that the energy levels changes in InAs/GaAs QDs due to the piezoelectric effects are quite small.³¹ Because the lattice mismatch in the InAs/InP QDs is only half of that of the InAs/GaAs QDs, we expect that the piezo-effect should be even smaller in the InAs/InP dots, and therefore is ignored in the present calculations.

The exciton energies are calculated using the configuration interaction (CI) method following Ref. 32.

III. STRAIN PROFILES AND STRAIN MODIFIED BANDOFFSETS

We first compare the strain profiles in the InAs/GaAs and the InAs/InP QDs. Figure 1 (a), (b) depict the hydrostatic and biaxial strain along the [100] direction and the [001] direction respectively for the InAs/GaAs dot, whereas Fig. 2 (a), (b) depict the strain profiles for the InAs/InP quantum dots. The strain is calculated for the lens-shaped QDs with $D=25$ nm, and

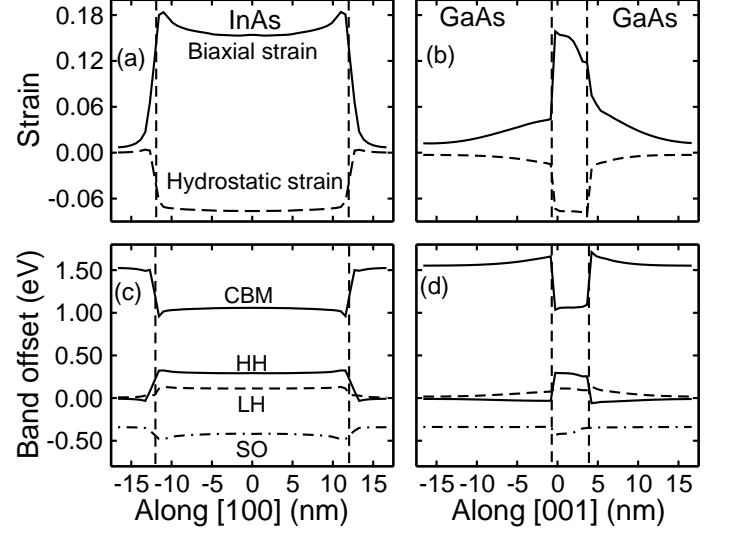


FIG. 1: Strain profiles and strain modified band-offsets for lens-shaped InAs/GaAs QD ($D=25$ nm, $h=3.5$ nm). The strain profiles are shown in (a) along the [100] direction and in (b) along the [001] direction. The strain modified band-offsets are shown in (c) along the [100] direction and in (d) along the [001] direction for the CBM, HH, LH and SO bands. The reference energy is chosen to be the VBM of GaAs.

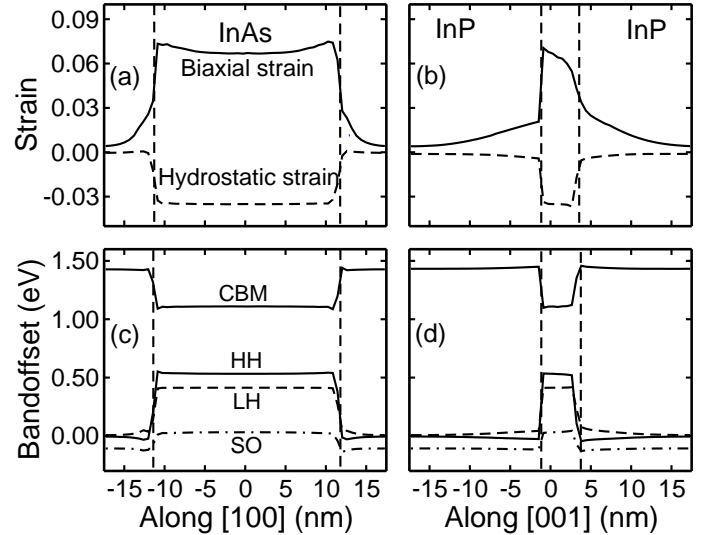


FIG. 2: Strain profiles and strain modified band-offsets for lens-shaped InAs/InP QD ($D=25$ nm, $h=3.5$ nm). The strain profiles are shown in (a) along the [100] direction and in (b) along the [001] direction. The strain modified band-offsets are shown in (c) along the [100] direction and in (d) along the [001] direction for the CBM, HH, LH and SO bands. The reference energy is chosen to be the VBM of InP.

$h=3.5\text{nm}$. The hydrostatic(isotropic) strain is defined as $I = \text{Tr}(\epsilon) = \epsilon_{xx} + \epsilon_{yy} + \epsilon_{zz}$, reflecting the relative change of volume i.e., $I \sim \Delta V/V$, whereas the biaxial strain is defined as $B = \sqrt{(\epsilon_{xx} - \epsilon_{yy})^2 + (\epsilon_{zz} - \epsilon_{xx})^2 + (\epsilon_{yy} - \epsilon_{zz})^2}$. As we can see, the hydrostatic strains of the InAs/InP and InAs/GaAs dots have very similar features: both are almost constants inside the dots and decay rapidly to zero in the matrices. The hydrostatic strain is negative in both dots, suggesting that the InAs dot is compressed. However, the hydrostatic strain in the InAs/InP dot is about half of that in the InAs/GaAs dot. The biaxial strain of both QDs also has similar features, decaying fast in the [100] and [010] directions outside the dots, it has long tails along the [001] direction.

The hydrostatic strain and the biaxial strain will shift the conduction band minimum (CBM) and the valence band maximum (VBM), and therefore modify the band-offsets of the QD. The biaxial strain will further split the heavy-hole (HH) and light-hole (LH) bands. We analyze the strain-modified band-offsets via Pikus-Bir model,^{33,34,35,36} using the local strain input from VFF calculations. This model, however, serves only as an illustration of the strain effect and is not used in our actual calculation of the single particle energy levels. The strain modified band-offsets are illustrated in Fig. 1 (c),(d) for InAs/GaAs quantum dot, and in Fig. 2 (c),(d) for InAs/InP quantum dot along the [100] direction and [001] direction respectively. The VBM of the unstrained host materials is set to be zero as the reference energy. The band-offsets in the InAs/GaAs dot are 480 meV for the electron and 280 meV for the hole, compared with 1050 meV for the electron and 46 meV for the hole in the unstrained system.³⁷ The confinement potential for electrons is stronger than that for holes. In contrast, for the unstrained InAs/InP system, the band-offset³⁷ is 580 meV for the electron and 420 meV for the hole, which change to 320 meV and 530 meV respectively in the InAs/InP QDs, due to the strain effects. The confinement potential for holes is stronger than that for electrons.¹⁴ Therefore, the confinement potentials in the InAs/GaAs and the InAs/InP QDs are very different. While the confinement for electrons is weaker in the InAs/InP QDs, the confinement for holes is significantly stronger. How the different confinement potentials lead to different electronic structure in the two dot systems will be discussed in Sec. IV. It was pointed out in Ref. 35 that in the tall InAs/GaAs QD, the biaxial strain might develop hole traps that localize holes at the interface of the QDs. This is unlikely to happen in the InAs/InP QDs for two reasons. (i) The strain in the InAs/InP QDs is much smaller than in the InAs/GaAs QDs. (ii) The band-offset for holes in the InAs/InP QDs is much larger than in the InAs/GaAs QDs.

The biaxial strain splits the HH and LH bands in addition to shifting the VBM. HH is higher in energy than the LH band, i.e., $E_{hh} > E_{lh}$ inside both dots. The HH-LH splitting is about 180 meV for the InAs/GaAs QD and 120 meV for the InAs/InP QD. Outside the QD, the

heavy-light-hole splitting changes sign, i.e., $E_{hh} < E_{lh}$.³⁵ It is also interesting to note that the SO band inside the InAs/GaAs quantum dot is lower in energy than outside the QDs, while the opposite is true for the InAs/InP quantum dot, due to the large band-offsets between InAs and InP for holes.

IV. SINGLE-PARTICLE ENERGY LEVELS AND WAVEFUNCTIONS

In this section, we compare the pseudopotential calculated single-particle energy levels as well as the wavefunctions of the InAs/InP QDs to those of the InAs/GaAs QDs. The energy levels are compared in three scales: (i) The energy difference between the lowest electron state and highest hole state, which largely determines the exciton energies and is in the order of 1 eV, (ii) The intraband energy spacing which is in the order of a few tens meV. (iii) The intraband p level splitting due to the C_{2v} atomistic symmetry of the QDs, which is in the order of a few meV. The single-particle energy levels of the InAs/InP dots are summarized in Table. I, whereas the results for the InAs/GaAs dots can be found in Table I of Ref. 38. The results of the InAs/GaAs QDs are very similar to what was obtained in Ref. 21.

A. Confined states and wavefunctions

Figure 3(a) depicts the energy levels of all confined electron states and 6 highest confined hole states of the InAs/InP QDs for various sizes. As a reference, we show in Fig. 3(b) the lowest 6 confined electron levels and the highest 6 confined hole levels of a InAs/GaAs QD of $D=20\text{ nm}$, $h=2.5\text{ nm}$. The zero energy is chosen to be the VBM of the host materials. The confined electron (hole) states are defined to be the states whose energies are lower (higher) than the CBM (VBM) of the host materials. We also show the electron and hole envelope wavefunctions of the InAs/GaAs and InAs/InP QDs for two dot geometries: a flat dot ($D=25\text{ nm}$, $h=2.5\text{ nm}$) in Fig. 4 (a) (b) and a tall dot ($D=25\text{ nm}$, $h=5.5\text{ nm}$) in Fig. 4 (c) (d). We show the lowest 6 electron and the highest 6 confined hole states for each dot. In all cases, the isosurface is chosen to enclose 50% of the total charge. The number on the bottom of each small panel gives the percentage of the density localized inside the QD.

1. Confined electron states

As we can see from Fig. 3, the InAs/InP QDs have fewer confined electron states compared to the InAs/GaAs QDs due to the smaller conduction band offset. In the smaller InAs/InP QD with $D=20\text{ nm}$, $h=2.5$

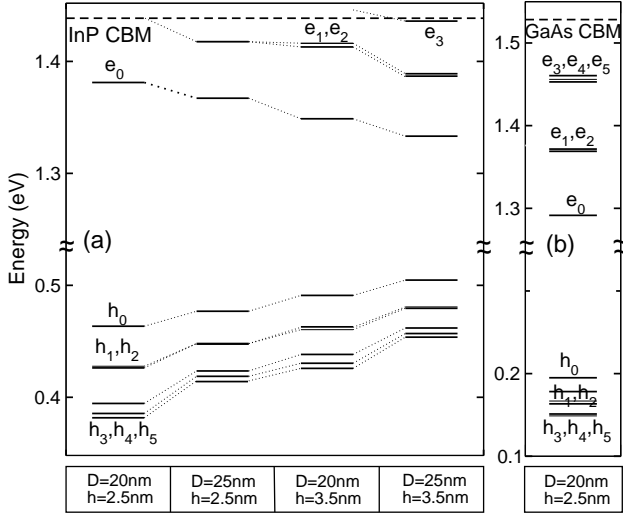


FIG. 3: Single-particle energy levels for (a) the lens-shaped InAs/InP QDs of different sizes, and (b) the lens-shaped InAs/GaAs QD ($D=20$ nm, $h=2.5$ nm). We show all confined electron states and the six highest confined hole states. The zero energies are chosen to be the VBM of the host materials.

nm, only one electron state (e_0) is confined. When we increase the dot base and height, more states are confined. For the dot with $D=25$ nm, $h=2.5$ nm, e_0 , e_1 and e_2 are confined, whereas in the dot with $D=25$ nm, $h=3.5$ nm, the e_4 and e_5 levels are also confined. The confined electrons show well defined s , p , d energy level shell structure in both the InAs/InP and the InAs/GaAs dots.

For the InAs/GaAs QDs, the electron wavefunctions of the flat dot [See Fig. 4 (a)] and the tall dot [See Fig. 4 (c)] have very similar shapes. The lowest state has s -like wavefunction, followed by 2 p -like states. The lower energy p orbital (e_1) has peaks along the $[1\bar{1}0]$ direction, whereas the higher energy p orbitals (e_2) has peaks along the $[110]$ direction.³⁹ Considering the next three levels, close in energy, the first two orbitals (e_4 , e_5) that have similar shapes are d orbitals, whereas the third orbital (e_5) having a peak in the dot center, is the $2s$ orbital. The wavefunctions of the InAs/InP dots have very similar shapes to the corresponding ones of the InAs/GaAs dots, except that the wavefunctions of the InAs/InP dots are larger, indicating that the electrons are less confined in the InAs/InP dots. In the flat InAs/InP QD, only about 53% of e_0 state is confined in the dot compared to 78% in the InAs/GaAs QD of the same size. Even in the tall InAs/InP QD, less than 82% of the e_0 state is confined compared to 92% in the tall InAs/GaAs QD.

2. Confined hole states

The valence band offset for the InAs/InP QDs is about 530 meV, which is almost twice as much as in the InAs/GaAs QDs. Therefore, more hole states are confined in the InAs/InP dots than in the InAs/GaAs dots. Unlike the InAs/GaAs dot, where the energy level shell structure for holes are not so obvious,³⁸ the InAs/InP dots have well defined hole s , p , d energy level shell structure, similar to those of electrons.

The shape of the hole wavefunctions in the InAs/GaAs dot is more complicate than that of the electron wavefunctions. But nevertheless in the flat dot [See Fig. 4 (a)] they can still be recognized as s , p , d , $2s$ orbitals although with some mixed characters.³⁵ In the tall InAs/GaAs dot, the holes are strongly localized on the interface of the dot due to the strain effects,³⁵ and do not have clear s , p , d characters any more [See Fig. 4 (c)]. On the other hand, the hole wavefunctions of the InAs/InP dots are quite different from those of the InAs/GaAs dots. They are quite similar to the electron wavefunctions, for both the flat and tall dots, except that the two p orbitals switch order in energy, i.e., the first hole p orbital has peaks along the $[110]$ direction, whereas the second hole p orbital has peaks along the $[1\bar{1}0]$ direction. The rotation of the p orbitals has also been noticed by Sheng et al.,¹² and was attributed to the piezoelectric effects. However, in our calculations, the piezo-effect is ignored, and therefore it cannot be the reason for the p orbital rotation. The rotation of the wavefunctions can be explored experimentally via magnetocapacitance spectroscopy.⁴⁰ Unlike in the InAs/GaAs dots, no hole localization has been found in the InAs/InP dots, because of their smaller strain and the large confinement potential for holes, as is discussed in Sec. III.

The holes are strongly confined in the InAs/InP QDs. Even in a small InAs/InP QD, more than 80% of charge density is localized in the QD for the h_0 and $h_{1,2}$ states. As a result, in a small InAs/InP QD, electrons could escape from the dot much more easily than holes, resulting in a positively charged system. Therefore the InAs/InP dot might be a good candidate for a memory device via hole storage in the dot.^{14,41,42}

3. Single-particle electron-hole energy gap

The single-particle electron-hole energy gap $\Delta\epsilon_{e,h} = e_0 - h_0$ is summarized in Table I. For the InAs/InP QDs with $D=20$ nm, and $h=2.5$ nm, $\Delta\epsilon_{e,h} \sim 917$ meV, which is about 180 meV less than that of the InAs/GaAs dot of the same size. The electron energy levels move down in energy, whereas the hole energy levels move up in energy, with the increasing of the base and height of the dot, as shown in Fig. 3 (a). As a result, $\Delta\epsilon_{e,h}$ decreases with the increasing of the dot size, due to the reduced confinement. For the dot of $D=20$ nm, $\Delta\epsilon_{e,h}$ changes from 918 meV at $h=2.5$ nm, to 798 meV at $h=5.5$ nm, with a 120 meV

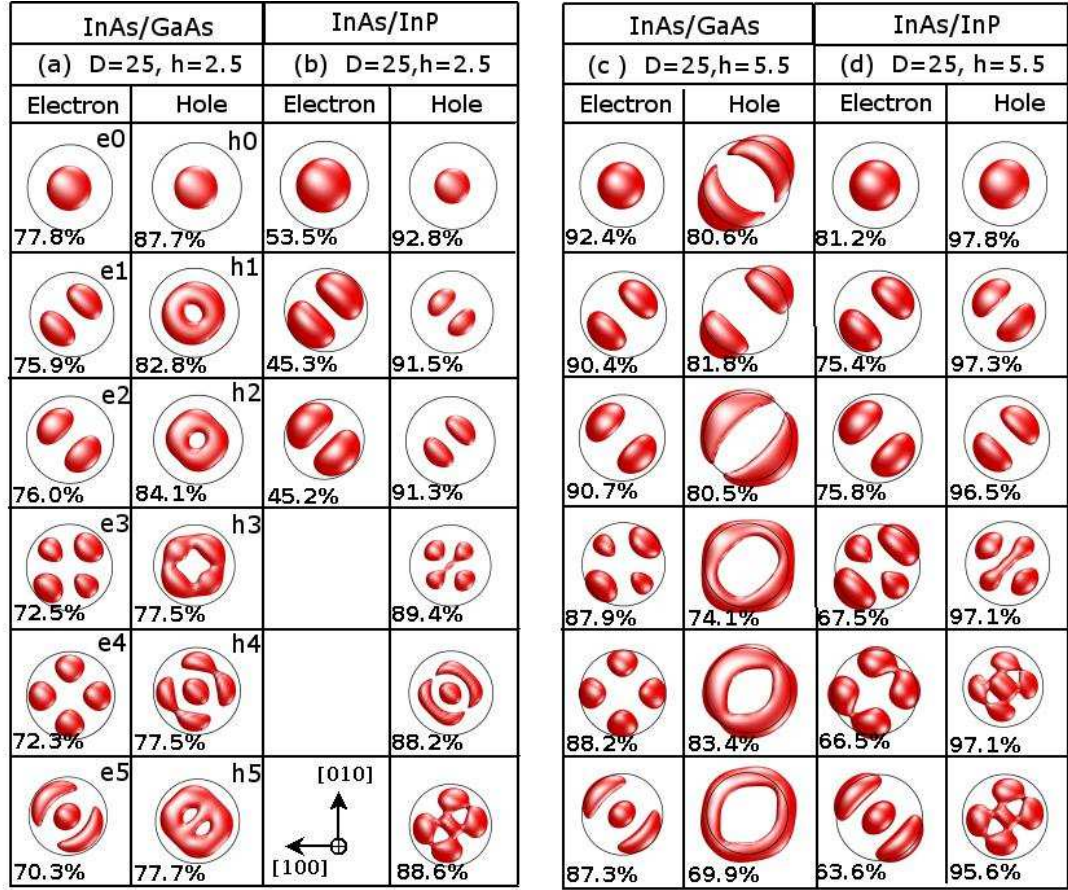


FIG. 4: (Color online) Top view of the squared wavefunctions of the confined electron and hole states for the InAs/GaAs and InAs/InP QDs. We show in (a), (b) the results of flat dots with $D=25$ nm, $h=2.5$ nm, and in (c) and (d) the results of tall dots with $D=25$ nm, $h=5.5$ nm. The isosurface is chosen to enclose 50% of the density. The number on the bottom of each small panel gives the percentage of the density localized inside the QD.

reduction. A similar $\Delta\epsilon_{e,h}$ reduction has been found for the InAs/InP dots of base $D=25$ nm when the dot height increases from 2.5 nm to 5.5 nm. The electron-hole energy gap reduction results in a corresponding redshift of the exciton emission lines (Sec. V).

B. Intraband energy spacings

The intraband energy spacing can be used to characterize the confinement effects in the QDs. We summarize the s - p energy spacing $\delta_{sp} = e_1 - e_0$ (or $h_0 - h_1$), and p - d energy level spacing $\delta_{pd} = e_3 - e_2$ (or $h_2 - h_3$) of the InAs/InP dots in Table I, whereas the results for the InAs/GaAs dots can be found in Table I of Ref. 38. To further see the trend of how the energy spacing changes with the dot size, we plot δ_{sp} of both InAs/GaAs and InAs/InP QDs, as a function of the dot height in Fig. 5 (a), (b) for electrons and holes respectively.

(a) *electrons*: The electron energy spacing of the InAs/InP dots is in the range of 50 to 70 meV, slightly

smaller than the energy spacing (50 to 80 meV) of the InAs/GaAs dots, due to the weaker confining potential for electrons in the InAs/InP dots. The s - p energy spacing δ_{sp} and p - d energy spacing δ_{pd} are nearly equal, in rough agreement with the EMA with harmonic confinements.

Intuitively, δ_{sp} should decrease monotonically by increasing the dot height. This trend is followed by the InAs/GaAs dots. Surprisingly, the electron δ_{sp} of the InAs/InP dots increases with the increasing of the dot height, against the naive expectation. In this case, both s , p levels move down in energy with the increasing of the dot size, but the s level moves down faster than the p levels,⁴³ leading to a larger δ_{sp} .

(b) *holes*: The hole energy spacing in the InAs/InP dots ranges from 20 to 40 meV, significantly larger than that (< 20 meV) of the InAs/GaAs dots of the same size. This is because the hole confining potential in the InAs/InP dots is about 340 meV larger than in the InAs/GaAs dots. Nevertheless, in all the InAs/InP QDs we have studied, the electron energy spacing is still about

TABLE I: Summary of the pseudopotential-calculated single-particle level spacing (in meV) of the InAs/InP quantum dots of different base sizes and heights (in nm). Unconfined states are leave in blank in the table.

	$D=20$				$D=25$			
	$h=2.5$	3.5	4.5	5.5	$h=2.5$	3.5	4.5	5.5
$e_1 - e_0$	56.6	64.1	67.4	67.9	49.1	53.6	56.0	55.7
$e_2 - e_1$		3.2	4.4	4.9	1.4	2.2	2.9	3.4
$e_3 - e_2$				61.1		48.0	52.6	53.8
$e_4 - e_3$							2.2	2.8
$e_5 - e_4$							3.5	5.3
$h_0 - h_1$	37.2	30.6	27.8	25.7	29.6	25.2	23.1	21.3
$h_1 - h_2$	1.5	2.5	3.5	4.2	0.7	1.2	1.5	1.7
$h_2 - h_3$	31.8	22.1	16.1	13.2	23.7	17.6	14.9	13.6
$h_3 - h_4$	9.0	7.9	6.6	4.4	4.8	4.9	4.9	4.2
$h_4 - h_5$	3.8	4.6	6.0	8.2	4.0	3.2	2.9	3.4
$e_0 - h_0$	917.7	857.8	821.1	798.4	890.3	828.7	791.1	768.5

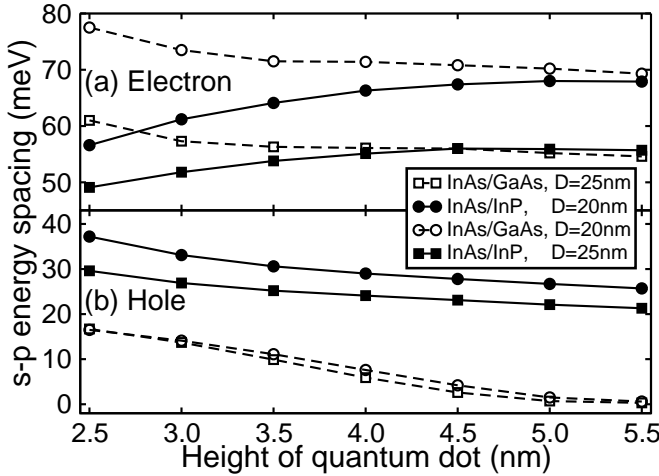


FIG. 5: Comparison of the intraband energy spacing δ_{sp} between the InAs/InP and InAs/GaAs QDs for (a) electrons, and (b) holes.

twice larger than that of the holes, because electrons have a much lighter effective mass than holes. For holes, δ_{pd} is much smaller than δ_{sp} , deviating from the harmonic potential approximation. As shown in Fig. 5 (b), the energy spacing δ_{sp} of holes decrease monotonically with the increasing of the dot height for both InAs/GaAs and InAs/InP QDs. No anomaly is found. Notice that for very tall QDs, δ_{sp} becomes very small for the InAs/GaAs QDs, due to the hole localization on the interface of the QDs [see Fig. 4 (c)], which is not the case for the InAs/InP QDs.

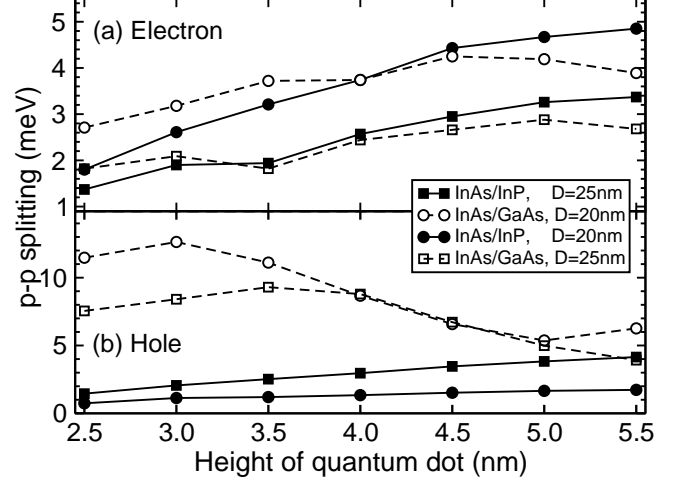


FIG. 6: Comparison of the p level splitting δ_{pp} between the InAs/InP and InAs/GaAs QDs for (a) electrons, and (b) holes.

C. Intraband p level splitting

In a continuum model, ignoring the underlying atomistic structure, a cylindrical QD has the $C_{\infty v}$ symmetry, leading to degenerate p , d levels. In contrast, the atomistic theories maintain the real symmetry of the QDs. For example, the lens-shaped QDs made of zinc-blende III-V semiconductors are of C_{2v} symmetry,³¹ where the $[110]$ and $[\bar{1}\bar{1}0]$ directions are non-equivalent, resulting in split p levels and d levels. The values of the p - p splitting $\delta_{pp} = e_2 - e_1$ (or $h_1 - h_2$) are summarized in Table I for the InAs/InP QDs. We also depict the p - p splittings as functions of dot height for both InAs/InP and InAs/GaAs QDs in Fig. 6.

1. p level splitting for electrons

The electron p - p splittings are shown in Fig. 6 (a) as functions of the dot height. The electron δ_{pp} is $\sim 1 - 2$ meV for flat InAs/InP dot, and increases to about 3 - 5 meV for the tall dots. The dots with the smaller base ($D=20$ nm) show a much larger p - p splitting. The electron p - p splitting for the InAs/InP dots is about 3%-5% of the electron s - p energy spacing δ_{sp} . The electron p - p splittings for the InAs/GaAs dots are in the range of 2 - 4 meV, and 3 % - 4% of δ_{sp} , and show a weak dependence on the dot height.

2. p level splitting for holes

The hole p - p splittings are shown in Fig. 6 (b). It has been shown in previous studies,^{21,38,44} that the hole p - p

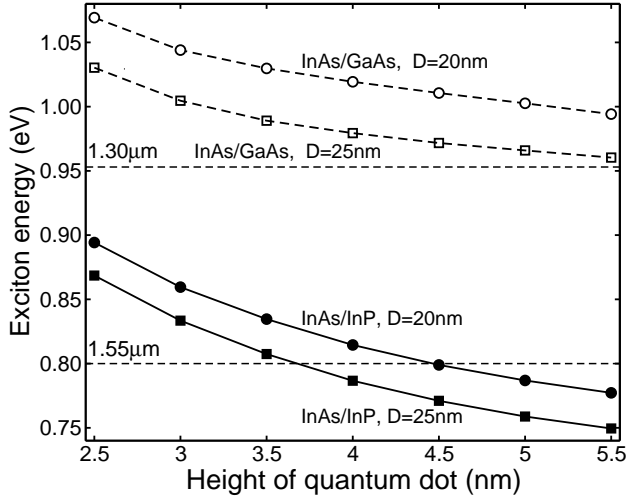


FIG. 7: Comparison of the primary exciton energies vs. dot height between the InAs/InP and InAs/GaAs QDs.

splittings can be larger than 10 meV in the InAs/GaAs dots, which is about 70% of the s - p energy spacing δ_{sp} . For very tall InAs/GaAs dots, in which the holes localize on the interface, δ_{pp} could even be much larger than δ_{sp} . The large p - p splitting leads to very different electronic and optical properties of the InAs/GaAs QDs than those predicted by continuum theories, e.g. the nontrivial charging pattern that breaks Hund's rule and the Aufbau principle for holes,^{38,44} that has been recently confirmed experimentally.^{27,45} Surprisingly, the calculated hole p - p splitting of the InAs/InP dot is much smaller than that of the InAs/GaAs dots, even though they have the same dot materials. For the flat InAs/InP dots, the splitting is only about 1 ~ 2 meV and for the tall dot with a small base ($D = 20$ nm) the splitting can be as large as 4.2 meV. Nevertheless, the hole δ_{pp} is less than 10 % of δ_{sp} for the InAs/InP dots. Therefore the multi-hole phase diagram and the charging patterns in the InAs/InP dots are expected to be very different from those in the InAs/GaAs dots, which can be examined by the hole charging experiments.²⁷ This is one of the most important results of the present work, which can not be obtained from the continuum theories. For example, a k - p theory predicted small (~ 1 meV) hole p - p splitting for both types of dots.^{12,46,47} The difference in the hole splitting for the two types of dots might come from their different strain profiles, the band offset, or the interface effects (common cation vs. common anion). We leave this for future investigations.

V. EXCITONS

Figure 7 depicts the fundamental exciton energies vs. dot height for the InAs/InP and InAs/GaAs dots. The exciton energies of the InAs/GaAs dots are about 200

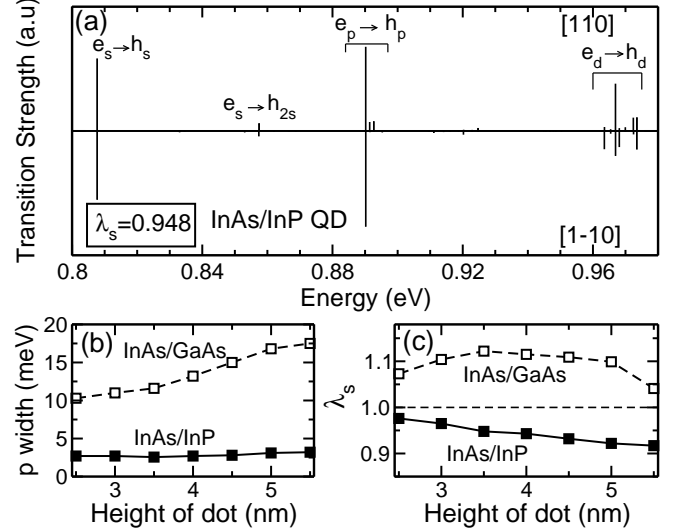


FIG. 8: (a) The exciton transition strengths for the InAs/InP QD of $D=25$ nm, $h=3.5$ nm. The upper panel is for the transitions polarized in the $[110]$ direction, while the lower panel is for transitions polarized in the $[1\bar{1}0]$ direction. λ_s is the polarization anisotropy (Eq. 3) of the S exciton. (b) The exciton P shell width vs. dot height. (c) The S exciton polarization anisotropy λ_s vs. dot height.

meV higher than those of the InAs/InP dots. The exciton energies decrease monotonically with increasing of the dot size. For the InAs/InP dot with $D=20$ (25) nm, the exciton energy reduces from about 900 (870) meV to about 780 (750) meV, as the dot height increases from 2.5 nm to 5.5 nm. The exciton energy reduction is about 120 meV, compared to 70 meV for the InAs/GaAs dots. One of the most important motivations of studying the InAs/InP dots is the 1.55 μm (~ 800 meV) emission for device applications. This wavelength can be easily achieved by the InAs/InP dots with a reasonable size, while it is challenging to be obtained using the InAs/GaAs dots, as shown in Fig. 7.

In the Hartree-Fock approximation, the fundamental exciton energy can be calculated as,

$$E_X = \Delta\epsilon_{e,h} - J^{(eh)}, \quad (2)$$

where $\Delta\epsilon_{e,h} = e_0 - h_0$ is the single-particle electron-hole energy gap and $J^{(eh)}$ is the direct electron-hole Coulomb energy. The electron-hole exchange energy is much smaller than $J^{(eh)}$ and therefore is ignored here. In typical InAs dots, $\Delta\epsilon_{e,h} \gg J^{(eh)}$. Therefore the exciton energy is largely determined by the single-particle electron-hole energy gap $\Delta\epsilon_{e,h}$ (See Sec: IV A 3).

We further calculated the higher excitonic transitions for the InAs/InP dot with $D=25$ nm and $h=3.5$ nm, for which the fundamental exciton wavelength is close to 1.55 μm . The results are shown in Fig. 8 (a), where the upper panel depicts the transition strength along the

[110] direction, while the lower panel shows the transition strength along the $[1\bar{1}0]$ direction. The transitions polarized along the [001] direction are about 4-5 orders of magnitude smaller than those parallel to the (001) plane, and are therefore not considered here. The excitonic transitions form several shells: the first shell coming from the e_0 to h_0 transitions is the exciton S shell. The transitions of $e_{1,2}$ to $h_{1,2}$, form the exciton P shell, whereas the transitions of $e_{3,4,5}$ to $h_{3,4,5}$ form the D shell.^{25,48} There is also a small transition peak at about 0.857 eV, which comes from the recombination of e_0 electron and h_5 hole. This transition, however, is significantly weaker in the InAs/GaAs QDs. The exciton P shell and D shell are composed of a bunch of transitions with slightly different transition energies. For the InAs/GaAs QDs, the width of the P shell is about 12 meV, whereas for the InAs/InP QD, the width is only about 2.5 meV. The D shell width is about 10 meV for the InAs/InP QDs, compared to about 22 meV in the InAs/GaAs dots. The P shell width with respect to the height of the QDs is presented in Fig. 8 (b) for the dot with $D=25$ nm. The P shell width of the InAs/GaAs increases to about 20 meV for $h=5.5$ nm. However, for InAs/InP dots, we found that the width is always about $2 \sim 3$ meV. This feature reflects the fact that the p level splitting is small for both electrons and holes in the InAs/InP dots, fact that could be examined by the single-dot optical spectroscopy.^{24,25}

We also calculated the light polarization anisotropy λ , defined as the ratio of the transition intensities along the [110] and $[1\bar{1}0]$ direction, i.e.,²¹

$$\lambda = \frac{I_{[110]}}{I_{[1\bar{1}0]}}. \quad (3)$$

The results for the S shell excitons in the dot with base $D=25$ nm are presented in Fig. 8 (c) for both the InAs/InP and InAs/GaAs dots. For the InAs/GaAs dot, we found $\lambda_s > 1$, indicating that the intensity along the [110] direction is stronger than that along the $[1\bar{1}0]$ direction,²¹ whereas, in the InAs/InP QD, $\lambda_s < 1$, indicating that the stronger intensity is along $[1\bar{1}0]$ direction. This feature could also be examined by the optical spectroscopy.

VI. CONCLUSION

We have studied the electronic structure of the InAs/InP QDs using an atomistic pseudopotential method and compared them to those of the InAs/GaAs QDs. Our results show that even though the InAs/InP QDs and InAs/GaAs QDs have the same dot material,

their electronic structure and optical properties differ significantly in certain aspects. These features, which may have important impacts for device applications, could be examined in future experiments. Some of the features can only be captured by atomistic theories and therefore provide a unique opportunity to test the predictive capability of the different theoretical approaches.

TABLE II: Band parameters obtained from the pseudopotential band structure and the target values of the fit. The “Target values” are conventional bulk parameters used in the literature (see Ref.37). ΔE_{VBO} is the valence band offset relative to the bulk InAs VBM. Δ_0 is the spin-orbit splitting, m^* are the effective masses at Γ , and a_g , a_v and b are the hydrostatic deformation potentials of the band gap, the valence band maximum, and the biaxial deformation potential of the valence band, respectively. The predicted band structure critical points are compared with the existing experimental data⁵⁰.

Parameters	InAs		InP	
	PP	Target	PP	Target
Fit				
E_g (eV)	0.410	0.410	1.424	1.424
ΔE_{VBO} (eV)	-0.006	0.000	-0.440	-0.420
Δ_0 (eV)	0.390	0.390	0.109	0.108
m_e^*	0.022	0.024	0.059	0.080
$m_{hh}^*(001)$	0.387	0.341	0.444	0.520
$m_{hh}^*(111)$	1.006	0.917	1.180	0.950
$m_{lh}^*(001)$	0.027	0.027	0.085	0.110
$m_{lh}^*(111)$	0.026	0.026	-	-
$m_{so}^*(001)$	0.097	0.085	0.152	0.21
a_g	-6.44	-6.6	-6.93	-6.0
a_v	-1.01	-1.0	-0.68	-0.6
b	-1.78	-1.70	-1.67	-2.0
Predictions				
Γ_{7c} (eV)	4.55	4.52	5.31	4.72
X_{6v}	-2.38	-2.4	-2.38	-2.3
X_{7v}	-2.37	-2.4	-2.25	-2.2
X_{6c}	2.28	-	2.21	2.38
X_{7c}	2.29	-	2.61	-
L_{6v}	-1.14	-0.90	-0.92	-1.23
$L_{4,5v}$	-0.87	-0.90	-0.80	-1.12
L_{6c}	1.46	-	2.15	2.03

APPENDIX A: EPM FOR INAS/INP

As explained in Sec. II the crystal potential is written as a superposition of atomic potentials v_α centered on the atomic positions. For each atomic potential we use for the screened pseudopotentials the expression proposed by Williamson et al.²¹

$$V_\alpha(r - R_{n\alpha}) = v_\alpha(r - R_{n\alpha}) [1 + \delta v_{n\alpha}(\epsilon)] = \frac{1}{\omega_c} \left(\sum_{\mathbf{q}} e^{i\mathbf{q} \cdot (r - R_{n\alpha})} v_\alpha(|\mathbf{q}|) \right) [1 + \delta v_{n\alpha}(\epsilon)], \quad (A1)$$

TABLE III: Fitted pseudopotential parameters for InAs/InP. A plane-wave cutoff of 5 Ryd is used.

parameters	As(In)	P(In)	In(As)	In(P)
α_0	56.8819	0.1509	853.4653	5012.0545
α_1	2.7023	2.9215	1.9724	1.8556
α_2	1.4894	1.2190	19.1236	88.8570
α_3	0.5757	0.3554	0.5439	0.7419
γ_α	0.00	0.00	1.6597	1.6460
α_{so}	0.1315	0.0140	0.4056	0.4800

where $v_\alpha(|\mathbf{q}|)$ has the functional form:

$$v_\alpha(|\mathbf{q}|) = a_{0\alpha} \cdot \frac{q^2 - a_{1\alpha}}{a_{2\alpha} e^{a_{3\alpha} q^2} - 1}, \quad (\text{A2})$$

and

$$\delta v_{n\alpha}(\epsilon) = \gamma_\alpha \cdot (\epsilon_{xx} + \epsilon_{yy} + \epsilon_{zz}). \quad (\text{A3})$$

ϵ_{ii} are elements of the local strain tensor. The term $\delta v_{n\alpha}(\epsilon)$ plays a crucial role in describing the absolute hydrostatic deformation potentials, in particular the variation of the valence band edge and, separately, the conduction band edge under arbitrary strains. This allows us to describe the modification of the valence and conduction band offsets when the systems are subjected to hydrostatic or biaxial deformation conditions such as in the case of epitaxial growth on a lattice-mismatched substrate. The parameters entering the previous equations have been determined by fitting a number of experimentally and theoretically (ab-initio) determined properties of bulk InP and InAs: the experimentally measured electron and hole effective masses, band gaps (target values at 0° K), and spin-orbit splittings, hydrostatic deformation potentials of the band gaps, band offsets, and LDA-predicted single band edge deformation potentials⁴⁹. In

the previous equation the term β has been introduced to represent the quasiparticle nonlocal self-energy effects. This kinetic energy scaling is needed to simultaneously fit bulk effective masses and band gaps.

In Table. II we report the target values we have fit for the binary InAs, and InP, and the results of the fitting procedure. The target values correspond to the band parameters used in the literature³⁷ at T = 0K. A 5 Ry kinetic cutoff was used when generating the pseudopotentials. This cutoff has then been used in the QD calculations of this paper. From Table II we see that the fit is satisfying. The corresponding parameters of the empirical pseudopotentials are given in Table III. Although we fitted only a few band properties per material, we checked that the fit works also for the full band structure. The predicted (not fitted) critical point energies are also reported in Table II. Notice that we are using slightly different potentials for the In atoms in InP and InAs, to take into account the different charge redistribution occurring around the In atom when it is placed in a different environment. Considering only the nearest-neighbor environment, the potential of each In atom in the structure is obtained as:

$$v_{\text{In}}(\text{As}_n\text{P}_{4-n}) = \frac{n}{4}v_{\text{In}}(\text{InAs}) + \frac{4-n}{4}v_{\text{In}}(\text{InP}) \quad (\text{A4})$$

ACKNOWLEDGMENTS

L.H. acknowledges the support from the Chinese National Fundamental Research Program, the Innovation funds and “Hundreds of Talents” program from Chinese Academy of Sciences, and National Natural Science Foundation of China (Grant No. 10674124). R. M. acknowledges support from the italian MIUR PRIN 2005.

- ¹ P. Caroff, C. Paranthoen, C. Platz, O. Dehaese, H. Folliot, N. Bertru, C. Labbé, R. Piron, E. Homeyer, A. L. Corre, et al., Appl. Phys. Lett. **87**, 243107 (2005).
- ² D. L. Huffaker, G. Park, Z. Zou, O. B. Shchekin, and D. G. Deppe, Appl. Phys. Lett. **73**, 2564 (1998).
- ³ G. Park, O. B. Shchekin, S. Csutak, D. L. Huffaker, and D. G. Deppe, Appl. Phys. Lett. **75**, 3267 (1999).
- ⁴ O. B. Shchekin and D. G. Deppe, Appl. Phys. Lett. **80**, 3277 (2002).
- ⁵ P. Michler, A. Kiraz, C. Becher, W. V. Schoenfeld, P. M. Petroff, L. Zhang, E. Hu, and A. Imamoglu, Science **290**, 2282 (2000).
- ⁶ O. Benson, C. Santori, M. Pelton, and Y. Yamamoto, Phys. Rev. Lett. **84**, 2513 (2000).
- ⁷ D. Loss and E. V. Sukhorukov, Phys. Rev. Lett. **84**, 1035 (2000).
- ⁸ M. Bayer, P. Hawrylak, K. Hinzer, S. Fafard, M. Korkusinski, Z. R. Wasilewski, O. Stern, and A. Forchell, Science **291**, 451 (2001).

- ⁹ D. L. Huffaker and D. G. Deppe, Appl. Phys. Lett. **73**, 520 (1998).
- ¹⁰ C. N. Allen, P. J. Poole, P. Marshall, J. Fraser, S. Raymond, and S. Fraser, Appl. Phys. Lett. **80**, 3269 (2002).
- ¹¹ D. Dalacu, D. Poitras, J. Lefebvre, P. J. Poole, G. C. Aers, and R. L. Williams, Appl. Phys. Lett. **84**, 3235 (2004).
- ¹² W. Sheng and P. Hawrylak, Phys. Rev. B **72**, 035326 (2005).
- ¹³ C. Cornet, A. Schliwa, J. Even, F. Doré, C. Celebi, A. Létoublon, E. Macé, C. Paranthoem, A. Simon, P. M. Koenraad, et al., Phys. Rev. B. **74**, 035312 (2006).
- ¹⁴ H. Pettersson, C. Pryor, L. Landin, M. E. Pistol, N. Carlsson, W. Seifert, , and L. Samuelson, Phys. Rev. B. **61**, 4795 (2000).
- ¹⁵ D. Chithrani, R. L. Williams, J. Lefebvre, P. J. Poole, and G. C. Aers, Appl. Phys. Lett. **84**, 978 (2003).
- ¹⁶ N. I. Cade, H. Gotoh, H. Kamada, H. Nakano, S. Anantathanasarn, and R. Nötzel, Appl. Phys. Lett. **89**, 181113 (2006).

- ¹⁷ E. D. P. Regreny, Y. Robach, M. Gendry, N. Chauvin, E. Tranvouez, G. Bremond, C. Bru-Chevallier, and G. Patriarche, *Appl. Phys. Lett.* **89**, 123112 (2006).
- ¹⁸ T. Ujihara, Y. Yoshida, W. S. Lee, and Y. Takeda, *Appl. Phys. Lett.* **89**, 083110 (2006).
- ¹⁹ M. Gendry, C. Monat, J. Brault, P. Regreny, G. Hollinger, B. Salem, G. Guillot, T. Benyattou, C. Bru-chevallier, G. Bremond, et al., *J. Appl. Phys.* **95**, 4761 (2004).
- ²⁰ L.-W. Wang and A. Zunger, *Phys. Rev. B* **59**, 15806 (1999).
- ²¹ A. J. Williamson, L.-W. Wang, and A. Zunger, *Phys. Rev. B* **62**, 12963 (2000).
- ²² S. Lee, L. Jönsson, J. W. Wilkins, G. W. Bryant, and G. Klimeck, *Phys. Rev. B* **63**, 195318 (2001).
- ²³ L. He, G. Bester, and A. Zunger, *Phys. Rev. Lett.* **94**, 016801 (2005).
- ²⁴ A. Kuther, M. Bayer, A. Forchel, A. Gorbunov, V. B. Timofeev, F. Schäfer, and J. P. Reithmaier, *Phys. Rev. B* **58**, R7508 (1998).
- ²⁵ P. Hawrylak, G. A. Narvaez, M. Bayer, and A. Forchel, *Phys. Rev. Lett.* **85**, 389 (2000).
- ²⁶ H. Drexler, D. Leonard, W. Hansen, J. P. Kotthaus, and P. M. Petroff, *Phys. Rev. Lett.* **73**, 2252 (1994).
- ²⁷ D. Reuter, P. Kailuweit, A. D. Wieck, U. Zeitler, O. Wibbelhoff, C. Meier, A. Lorke, and J. C. Maan, *Phys. Rev. Lett.* **94**, 026808 (2005).
- ²⁸ C. Paranthoen, N. Bertru, and O. Dehaese, *Appl. Phys. Lett.* **78**, 1751 (2001).
- ²⁹ P. N. Keating, *Phys. Rev.* **145**, 637 (1966).
- ³⁰ R. M. Martin, *Phys. Rev. B* **1**, 4005 (1970).
- ³¹ G. Bester and A. Zunger, *Phys. Rev. B* **71**, 045318 (2005).
- ³² A. Franceschetti and A. Zunger, *Europhys. Lett.* **50**, 243 (2000).
- ³³ G. E. Pikus and G. L. Bir, *Fiz. Tverd. Tela (Leningrad)* **1**, 154, (1959); **1**, 1642 (1959); **3**, 1001 (1961) [*Sov. Phys. Solid State* **1**, 136 (1959); **1**, 1502 (1959); **3**, 730 (1961)]; *Phys. Rev. Lett.* **6**, 103 (1961).
- ³⁴ S.-H. Wei and A. Zunger, *Phys. Rev. B* **49**, 14337 (1994).
- ³⁵ L. He, G. Bester, and A. Zunger, *Phys. Rev. B* **70**, 235316 (2004).
- ³⁶ C. Pryor, J. Kim, L.-W. Wang, A. J. Williamson, and A. Zunger, *J. Appl. Phys.* **83**, 2548 (1998).
- ³⁷ I. Vurgaftman, J. R. Meyer, and L. R. Ram-Mohan, *J. Appl. Phys.* **89**, 5815 (2001).
- ³⁸ L. He and A. Zunger, *Phys. Rev. B* **73**, 115324 (2006).
- ³⁹ We adopt the definition of the crystallographic direction of Ref. 31, which choose to place the cation at the origin (0,0,0). In Ref. 21, a different convention for the [110] direction has been used.
- ⁴⁰ O. S. Wibbelhoff, A. Lorke, D. Reuter, and D. Wieck, *Appl. Phys. Lett.* **86**, 092104 (2005).
- ⁴¹ S. Y. Verbin, B. Pal, M. Ikezawa, I. V. Ignatiev, and Y. Masumoto, *arXiv:cond-mat/0608043* (2006).
- ⁴² B. Pal, S. Y. Verbin, I. V. Ignatiev, M. Ikezawa, and Y. Masumoto, *arXiv:cond-mat/0702063* (2007).
- ⁴³ The p levels are slightly higher than the VBM of InP, and therefore are weakly confined when dot height $h < 3.5$ nm.
- ⁴⁴ L. He, G. Bester, and A. Zunger, *Phys. Rev. Lett.* **95**, 246804 (2005).
- ⁴⁵ G. Bester, D. Reuter, L. He, A. Zunger, P. Kailuweit, A. D. Wieck, U. Zeitler, J. C. Maan, O. Wibbelhoff, and A. Lorke, *unpublished*.
- ⁴⁶ S. Lee, O. L. Lazarenkova, P. vonAllmen, F. Oyafuso, and G. Klimeck, *Phys. Rev. B* **70**, 125307 (2004).
- ⁴⁷ W. Sheng, S. J. Cheng, and P. Hawrylak, *Phys. Rev. B* **71**, 035316 (2005).
- ⁴⁸ M. Bayer, O. Stern, P. Hawrylak, S. Fafard, and A. Forchel, *nature* **405**, 923 (2000).
- ⁴⁹ S.-H. Wei and A. Zunger, *Appl. Phys. Lett.* **72**, 2011 (1998).
- ⁵⁰ *Semiconductors: Group IV and III-V Compounds*, edited by O. Madelung, Landolt-Börnstein, New Series, Group III, Vol. 17, (Springer, Berlin, 1982); *Semiconductors: Intrinsic Properties of Group IV Elements and III-V, II-VI and I-VII Compounds*, edited by O. Madelung, Landolt-Börnstein, New Series, Group III, Vol. 22, (Springer, Berlin, 1987).